

Supporting Information

Encapsulating the ionic liquids into POM-based MOFs to improve their conductivity for superior lithium storage

Mi Zhang,^{‡a} A-Man Zhang,^{‡a}, Xiao-Xiao Wang,^a Qing Huang,^a Xiaoshu Zhu,^b Xiao-Li Wang,^a Long-Zhang Dong,^a Shun-Li Li^{*a} and Ya-Qian Lan ^{*a}

^a Jiangsu Collaborative Innovation Centre of Biomedical Functional Materials, Jiangsu Key Laboratory of New Power Batteries, College of Chemistry and Materials Science, Nanjing Normal University, Nanjing 210023, P. R. China

^b Center for Analysis and Testing, Nanjing Normal University, Nanjing 210023, P.R. China

*E-mail: yqlan@njnu.edu.cn

‡ These authors contribute equally to this work.

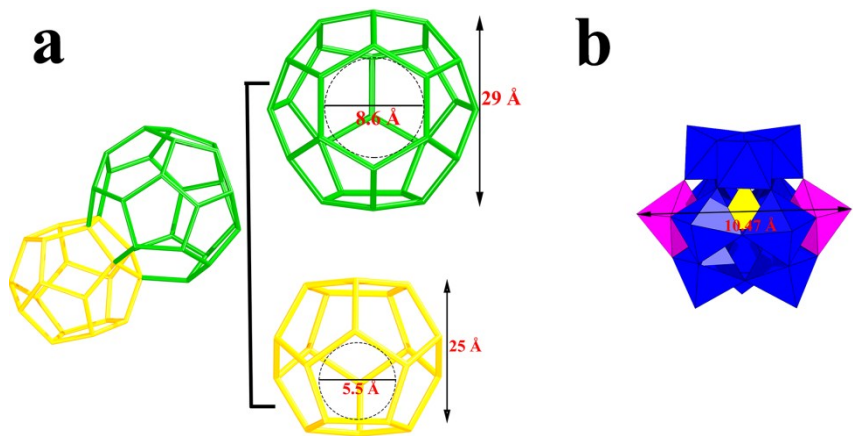


Fig. S1. (a) The two types of cages in polyhedral mode and the pentagonal and hexagonal windows of MIL-100, (b) Molecular structure of $\text{PMo}_{10}\text{V}_2$.

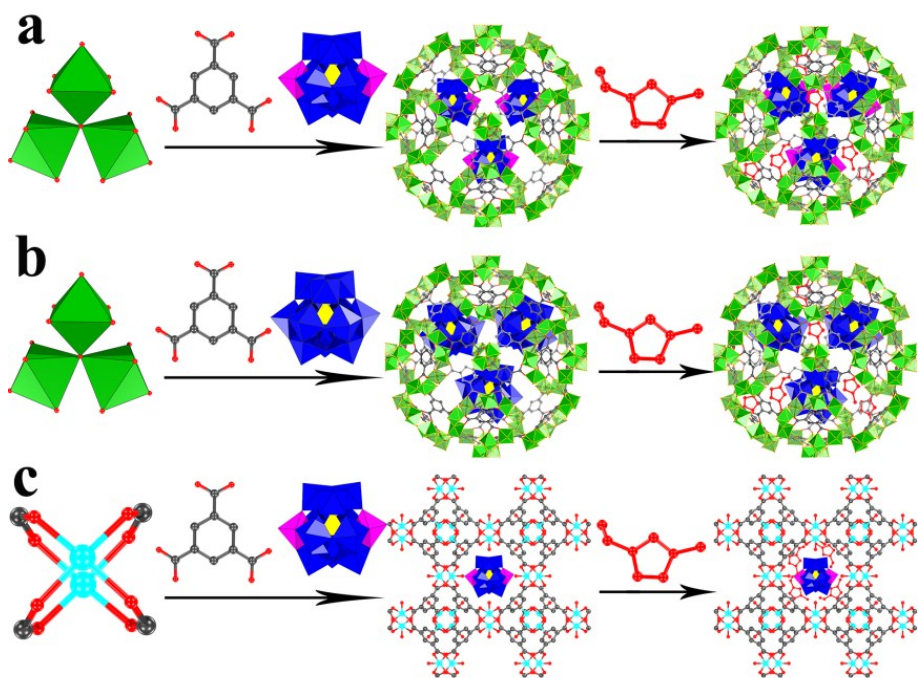


Fig. S2. (a) Schematic view of $\text{PMo}_{10}\text{V}_2\text{-ILs@MIL-100}$ crystals, (b) Schematic view of $\text{PMo}_{12}\text{-ILs@MIL-100}$ crystals, (c) Schematic view of $\text{PMo}_{10}\text{V}_2\text{-IL@HKUST-1}$ crystals.

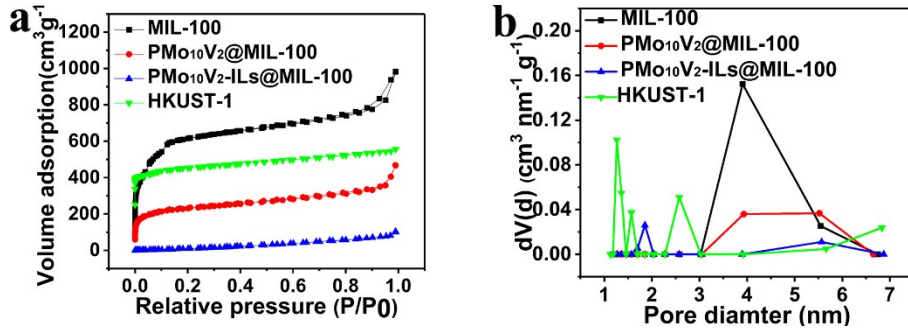


Fig. S3. (a) N₂ adsorption-desorption isotherms and pore size distributions of MIL-100, PMo₁₀V₂@MIL-100, PMo₁₀V₂-ILs@MIL-100 and HKUST-1 crystals.

Compared with the MIL-100, the PMo₁₀V₂@MIL-100 sample presents a significant decrease in surface area (from 1869.8 to 665 m²g⁻¹), in agreement with the presence of PMo₁₀V₂. The pores of PMo₁₀V₂@MIL-100 are further taken up by the ILs, resulting in a further reduction in surface area (84.08 m²g⁻¹). The BJH pore size distribution also reflects the volume changes during the encapsulation process. In addition, the MIL-100 exhibits a much larger surface area (1869.8 m²g⁻¹) and larger pore size distribution than the HKUST-1 (1346.352 m²g⁻¹).

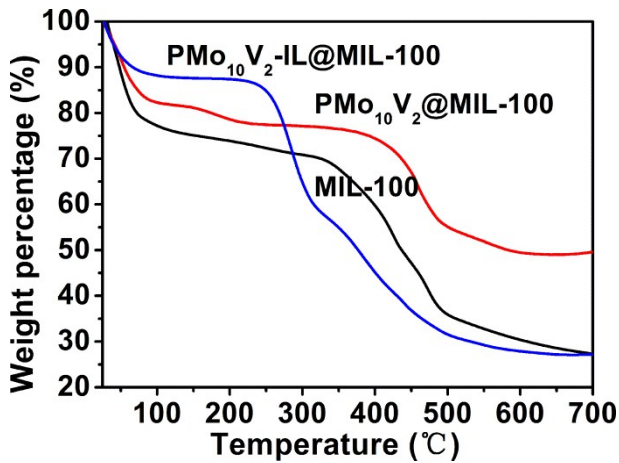


Fig. S4. TGA results of MIL-100, PMo₁₀V₂@MIL-100 and PMo₁₀V₂-ILs@MIL-100 crystals.

Compared with MIL-100, PMo₁₀V₂@MIL-100 and PMo₁₀V₂-ILs@MIL-100 crystals show less weight loss because of the encapsulation of PMo₁₀V₂ and PMo₁₀V₂-ILs at the beginning. The initial weight loss up to 80 °C related to the release of free water, while water interacted with the frameworks or PMo₁₀V₂ degrades between 80 and 200 °C. These samples further degrade at higher temperature (>270 °C) with the departure of the benzenetricarboxylate groups.

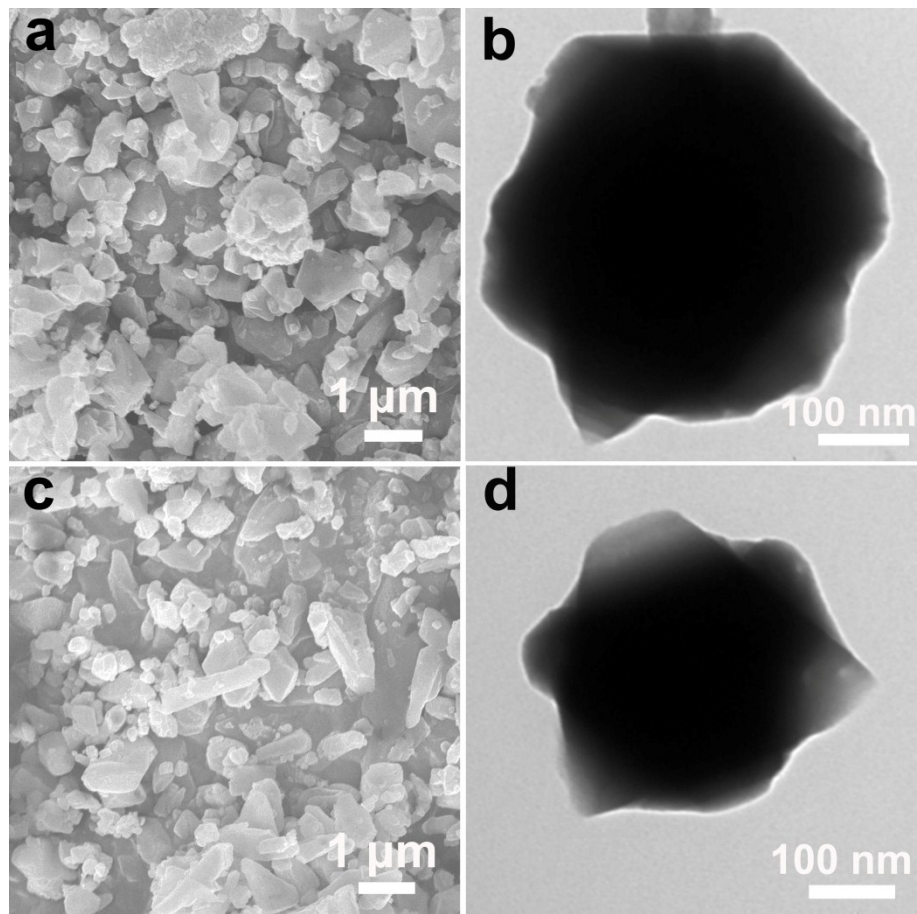


Fig. S5. (a) SEM image of MIL-100 crystals, (b) TEM image of MIL-100 crystals, (c) SEM image of $\text{PMo}_{10}\text{V}_2@\text{MIL-100}$ crystals, (d) TEM image of $\text{PMo}_{10}\text{V}_2@\text{MIL-100}$ crystals.

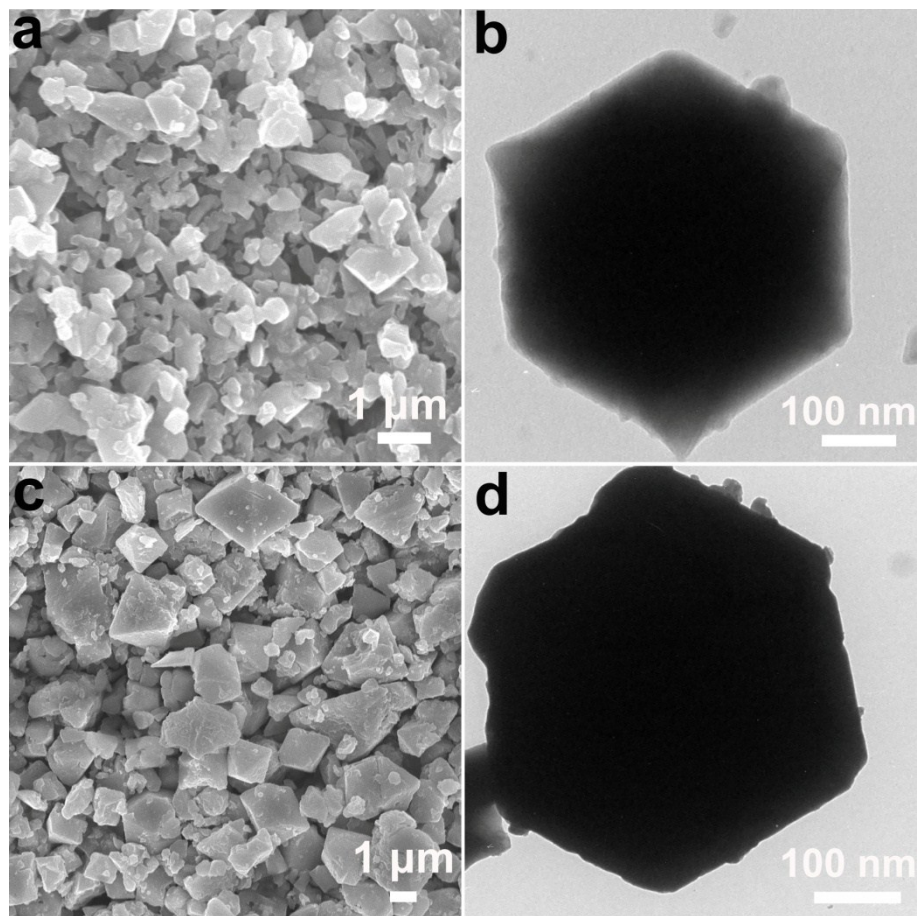


Fig. S6. (a) SEM image of $\text{PMo}_{12}\text{-ILs@MIL-100}$ crystals, (b) TEM image of $\text{PMo}_{12}\text{-ILs@MIL-100}$ crystals, (c) FE-SEM image of $\text{PMo}_{10}\text{V}_2\text{-ILs@HKUST-1}$ crystals, (d) TEM image of $\text{PMo}_{10}\text{V}_2\text{-ILs@HKUST-1}$ crystals.

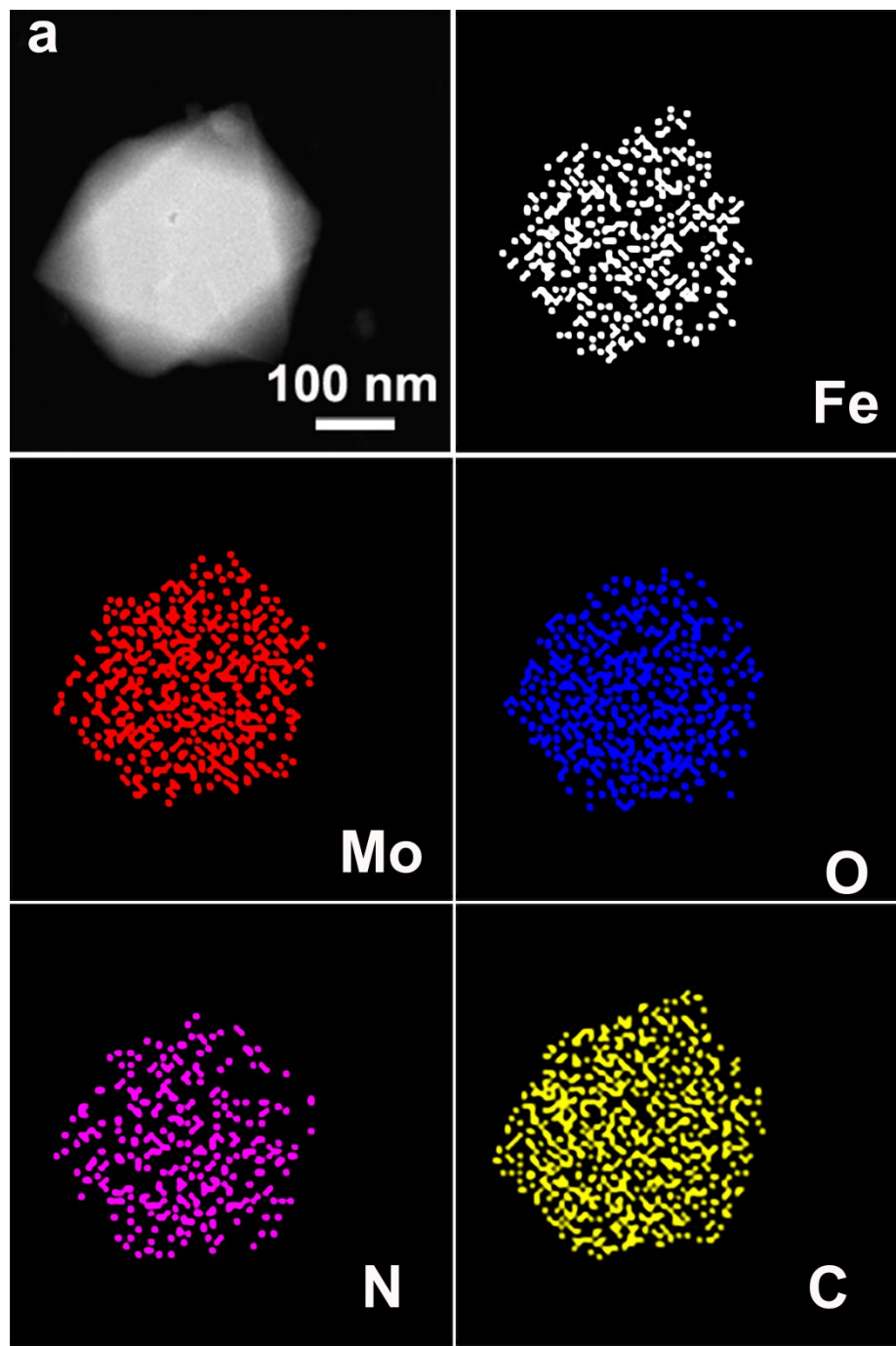


Fig. S7. STEM image of $\text{PMo}_{12}\text{-ILs@MIL-100}$ crystals and the corresponding mapping images of Fe, Mo, O, N and C.

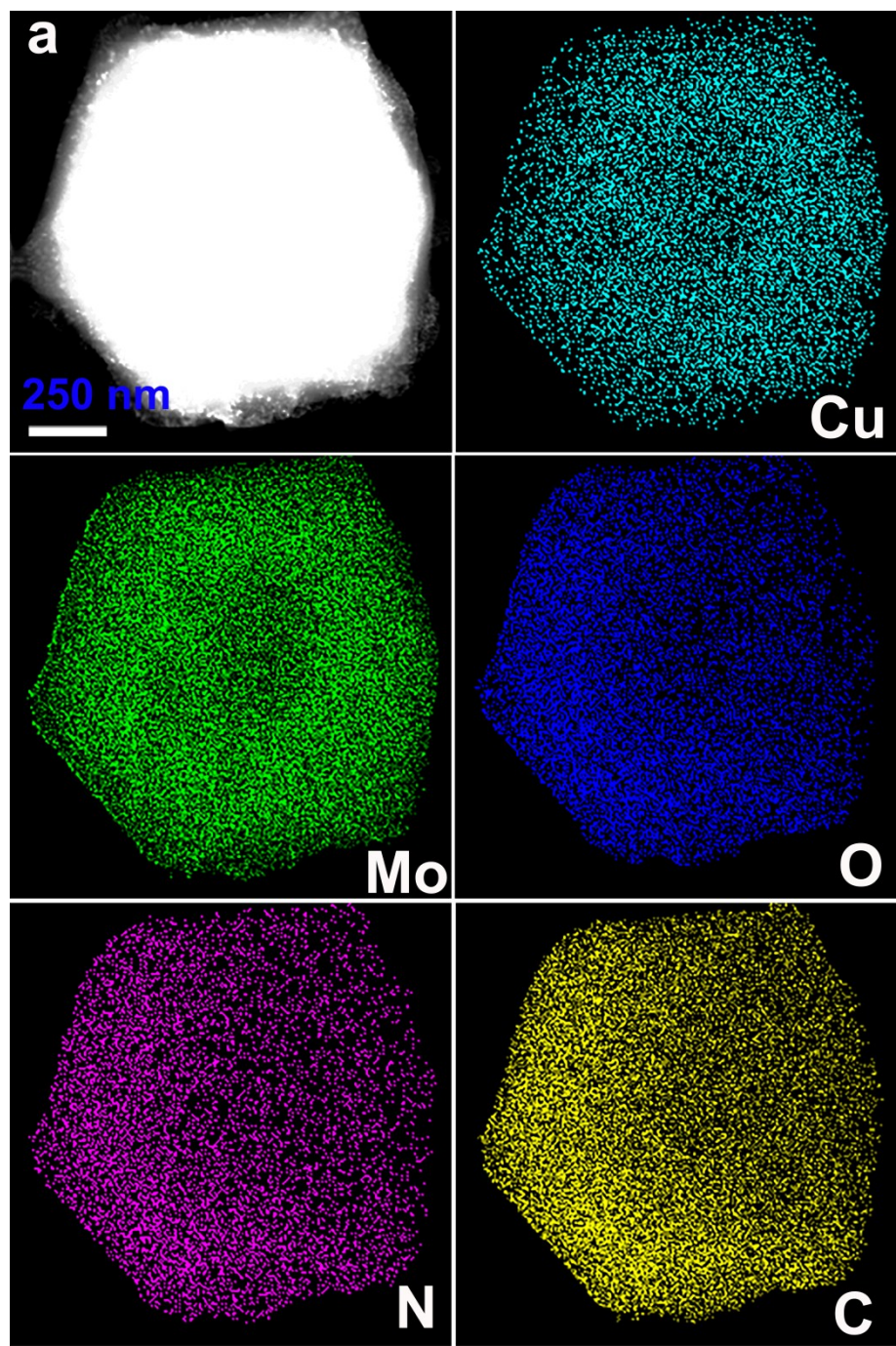


Fig. S8. STEM image of PMo₁₀V₂-ILs@HKUST-1 crystals and the corresponding mapping images of Cu, Mo, O, N and C.

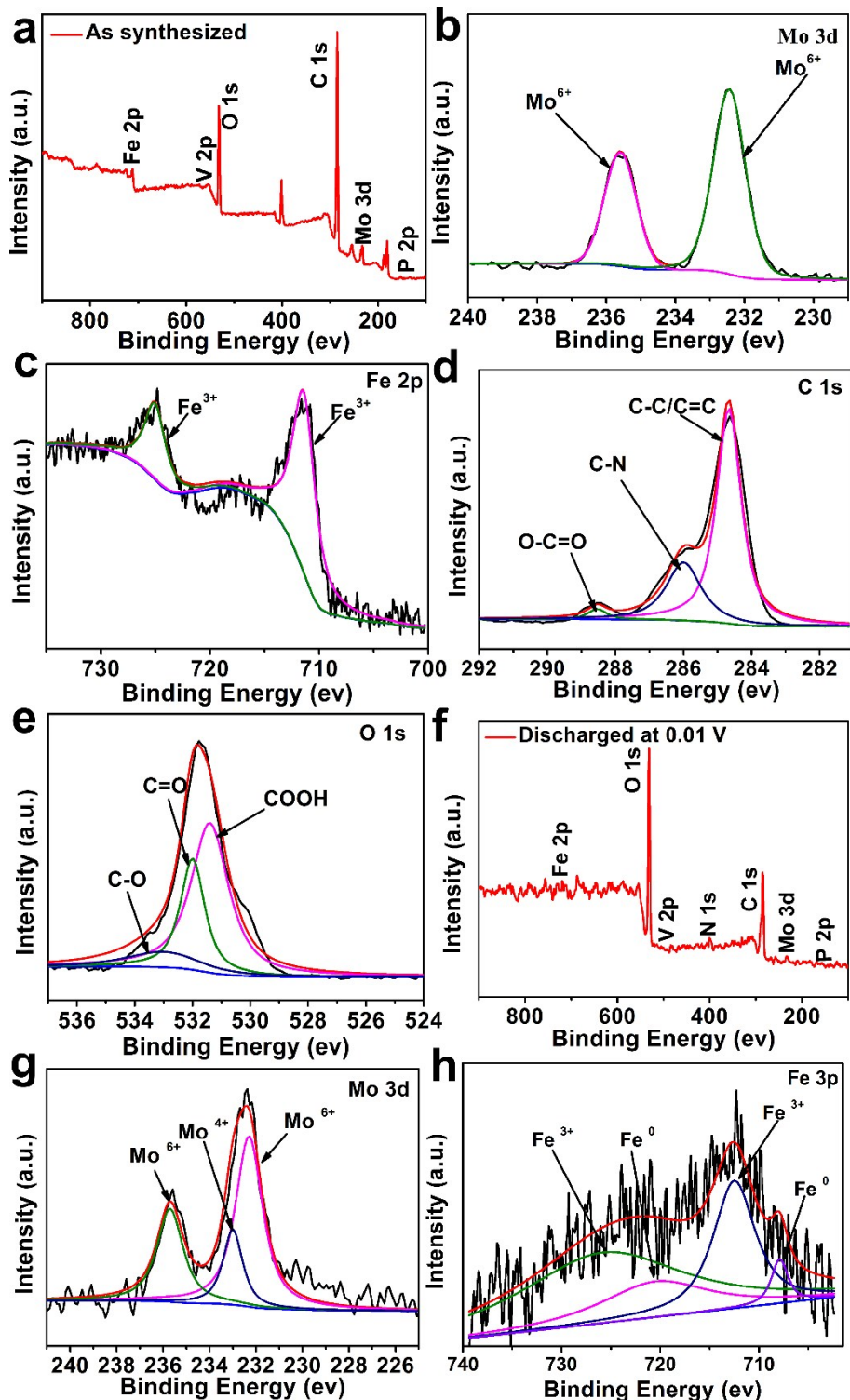


Fig. S9. XPS spectra of PMo₁₀V₂-ILs@MIL-100 crystals before and after discharged to 0.01 V, (a-e): As-synthesized powder (a) as-synthesized powder survey scan, (b) Mo 3d, (c) Fe 3p, (d) C 1s, (e) O 1s, respectively, (f-h): Discharged at 0.01 V, (f) survey scan (g) Mo 3d, (h) Fe 3p, respectively.

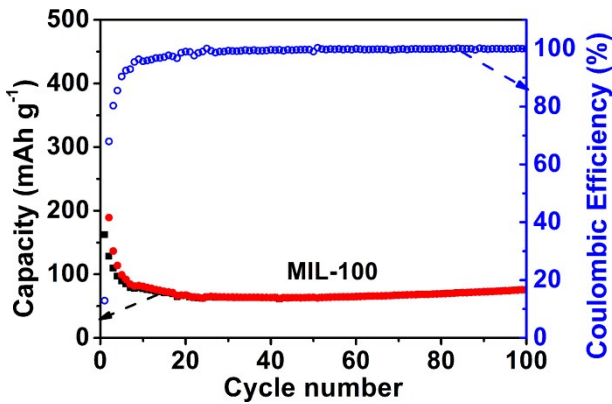


Fig. S10. Cycle-life performance of MIL-100 crystals at a current density of 0.1 A g^{-1} .

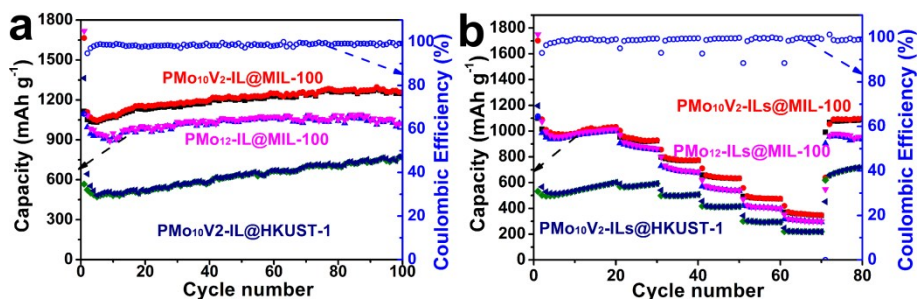


Fig. S11. (a) Cycle-life performance of $\text{PMo}_{10}\text{V}_2\text{-ILs@MIL-100}$, $\text{PMo}_{12}\text{-ILs@MIL-100}$ and $\text{PMo}_{10}\text{V}_2\text{-ILs@HKUST-1}$ crystals at a current density of 0.1 A g^{-1} , (b) Rate capability test for the $\text{PMo}_{10}\text{V}_2\text{-ILs@MIL-100}$, $\text{PMo}_{12}\text{-ILs@MIL-100}$ and $\text{PMo}_{10}\text{V}_2\text{-ILs@HKUST-1}$ crystals at various current densities ($0.1\text{-}3 \text{ A g}^{-1}$).

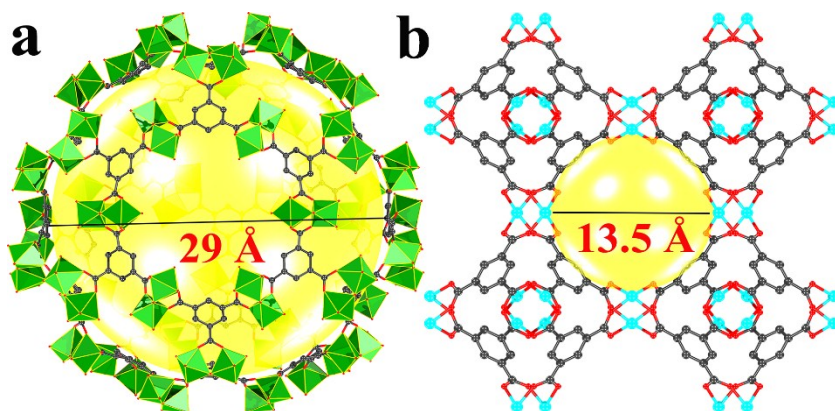


Fig. S12. (a) The corresponding simulated cages of MIL-100, (b) the corresponding simulated cages of HKUST-1.

Determination of diffusion coefficients

The diffusion coefficient values of the Li⁺ ions (D) can be calculated based on the EIS spectra by using the Eqs. (1) and (2),

$$D = 0.5 \left(\frac{RT}{n^2 F^2 A C} \right)^2 \quad (1)$$

$$Z' = R_D + R_L + \sigma \omega^{-1/2} \quad (2)$$

where R is the gas constant, T is the temperature, n is the number of electron transfer per molecule during intercalation, F is Faraday's constant, A is the area of the electrode surface, C is the molar concentration of Li⁺ ions, and σ is the Warburg factor. Based on the Eq. (2), the linear fitting of Z' and ω^{-1/2} is displayed in Fig. S9b.¹ From the fitting results, the σ value can be calculated for the slope. At the third cycles, the ratio of $\sigma_{PMo10V2-ILs@MIL-100}/\sigma_{PMo10V2@MIL-100}$ is 0.3318, corresponding to $D_{PMo10V2-ILs@MIL-100}/D_{PMo10V2@MIL-100} \approx 9.08$.

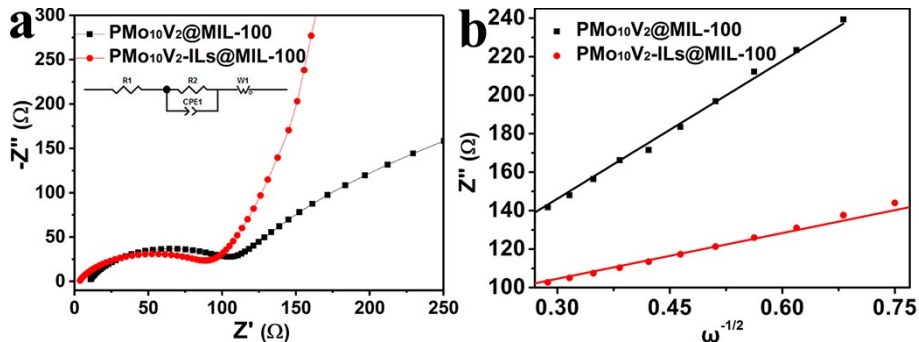


Fig. S13. (a) Nyquist plots of the PMo₁₀V₂@MIL-100, and PMo₁₀V₂-ILs@MIL-100 crystals after third cycles, (b) Z' vs. $\omega^{-1/2}$ plots.

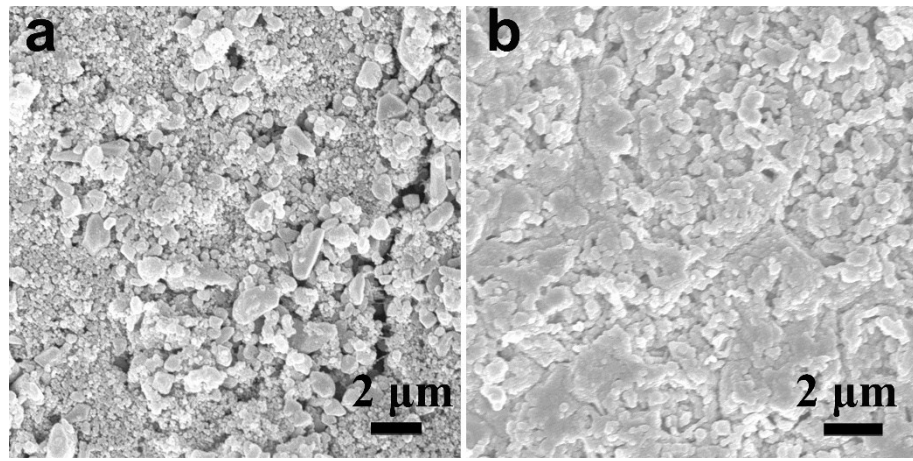


Fig. S14. SEM images of (a) PMo₁₀V₂-ILs@MIL-100 crystals electrode before and (b) after 100 cycles performed with a current density of 0.5 A g⁻¹.

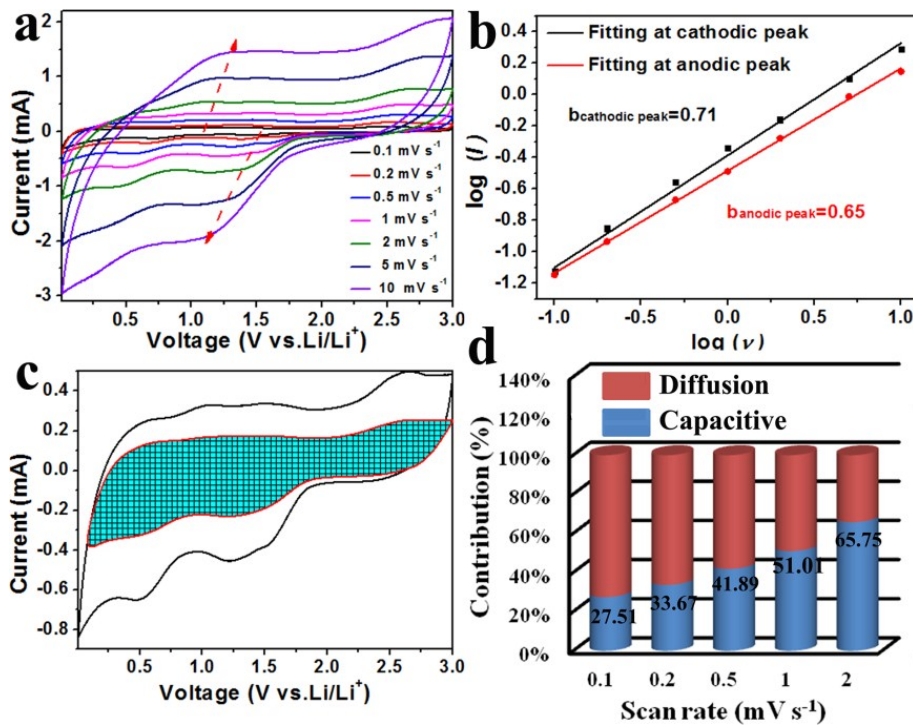


Fig. S15. (a) CV curves of PMo₁₀V₂-ILs@HKUST-1 crystals at various scan rates, from 0.1 to 10 mV s⁻¹, (b) b-value determination of cathodic and anodic peaks, (c) Capacitive-controlled charge storage contributions separated with cyclic voltammogram at 1 mV s⁻¹ scan, (d) Normalized contribution ratio of capacitive (blue) and diffusion-limited (red) capacities at various scan rates.

Table S1. Summary of various electrochemical parameters for PMo₁₀V₂@MIL-100, PMo₁₀V₂-ILs@MIL-100.

Sample	Rs (ohm)	Rct (ohm)	Conductivity (S·cm ⁻¹)
PMo ₁₀ V ₂ @MIL-100	9.79	89.2	3.13*10 ⁻¹⁰
PMo ₁₀ V ₂ -ILs@MIL-100	2.655	68.08	9.67*10 ⁻⁶

Table S2. The Fe and Mo contents of PMo₁₀V₂-ILs@MIL-100 crystals by ICP analysis.

Sample	w _{Fe} /mg L ⁻¹	n _{Fe} /umol L ⁻¹	w _{Mo} /mg L ⁻¹	n _{Mo} /umol L ⁻¹	Fe:Mo
PMo ₁₀ V ₂ -ILs@MIL-100	4.398	78.534	6.636	69.126	1.136

Table S3. The Cu and Mo contents of PMo₁₀V₂-ILs@HKUST-1 crystals by ICP analysis.

Sample	w _{Cu} /mg L ⁻¹	n _{Cu} /umol L ⁻¹	w _{Mo} /mg L ⁻¹	n _{Mo} /umol L ⁻¹	Cu:Mo
PMo ₁₀ V ₂ -ILs@HKUST-1	5.942	92.833	7.065	73.609	1.261

Table S4. The C, N and O contents in different samples by Elemental analysis.

Sample	C (n%)	N (n%)	H (n%)
PMo ₁₀ V ₂ -ILs@MIL-100	34.1	3.28	17.9
PMo ₁₀ V ₂ -ILs@HKUST-1	31.2	24.0	2.95

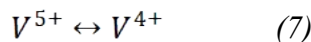
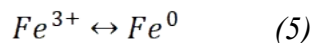
Calculation of the theoretical capacities:

The theoretical capacities were calculated according to equation (3):

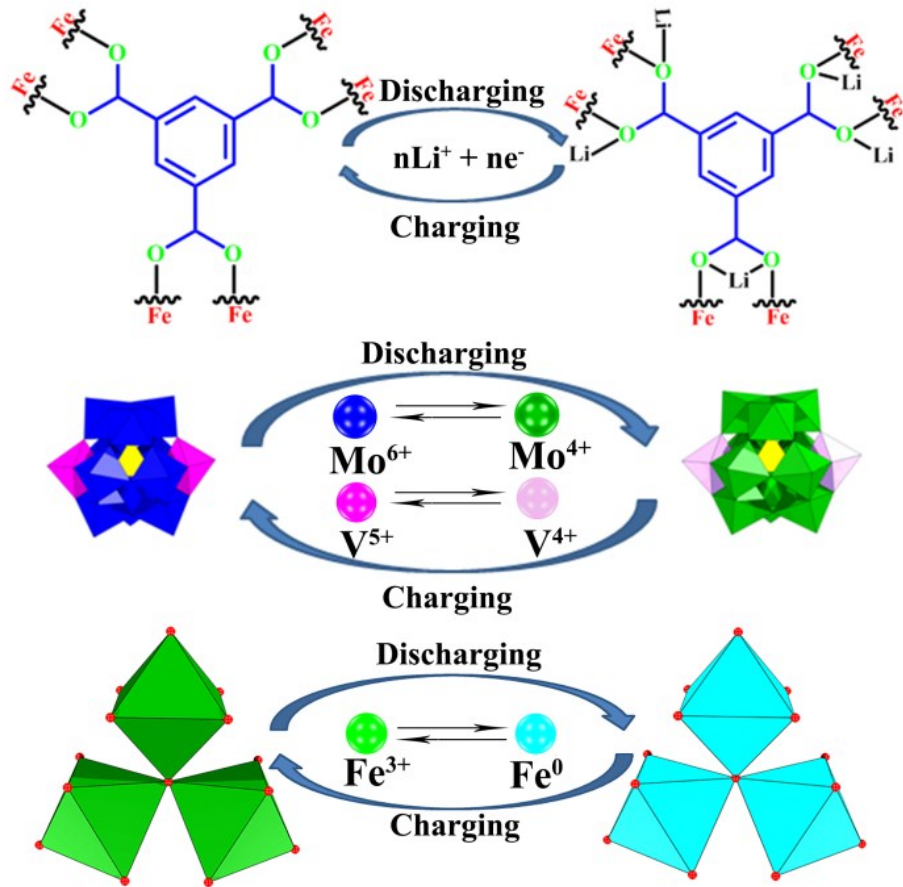
$$Q = \frac{nF}{3.6M} = \frac{96500F}{3.6M} \quad (4)$$

Where Q is the reversible charging–discharging capacity, n is the number of electrons passed during the redox reaction, and M is the molecular weight.

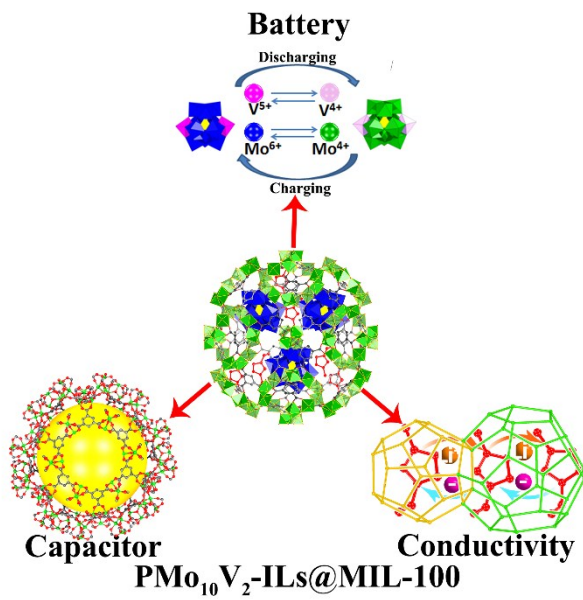
Owing to the intercalation mechanism for Li storage (equations 5-7), we consider the redox reactions of metal ions (Fe, Mo and V), which is also confirmed by the XPS results in Fig. S6.



According to the results of ICP analysis and Elemental analysis, we can speculate the molecular formula of $PMO_{10}V_2\text{-ILs@MIL-100}$ is $\{Fe_3O(H_2O)_2OH[C_6H_3(CO_2)_3]_2\}[PMo_{10}V_2O_{40}]_{0.2641}[C_6H_{11}N_2]_{1.213}$ and the molecular formula of $PMO_{10}V_2\text{-ILs@HKUST-1}$ is $\{Cu_2[C_6H_3(CO_2)_3]_{4/3}\}_6[PMo_{10}V_2O_{40}]_{0.9516}[C_6H_{11}N_2]_{4.875}$. If 2.641 Mo^{6+} , 0.5282 V^{5+} , and 3 Fe^{3+} ions in $PMO_{10}V_2\text{-ILs@MIL-100}$ are reduced to Mo^{4+} , V^{4+} and Fe^0 , respectively, and possible lithiation/delithiation sites for coordination with Li in the organic ligands, maximum of $n_{PMo10V2\text{-ILs@MIL-100}} = 26.8102$, $Q_{PMo10V2\text{-ILs@MIL-100}} = 601.68 \text{ mAh g}^{-1}$. If 9.516 Mo^{6+} , 1.9032 V^{5+} in $PMO_{10}V_2\text{-ILs@HKUST-1}$ are reduced to Mo^{4+} and V^{4+} , respectively, and possible lithiation/delithiation sites for coordination with Li in the organic ligands, maximum of $n_{PMO10V2\text{-ILs@HKUST-1}} = 68.9352$, $Q_{PMO10V2\text{-ILs@HKUST-1}} = 399.25 \text{ mAh g}^{-1}$.



Scheme S1. The schematic diagram of the possible mechanism for the theoretical capacities of $\text{PMo}_{10}\text{V}_2\text{-ILs@MIL-100}$ crystals.



Scheme S2. The schematic diagram of the possible mechanism for the synergistic effect of $\text{PMo}_{10}\text{V}_2\text{-ILs@MIL-100}$ crystals.

Table S5. Comparison of MOFs, POMs and POMOFs-based anodes in this work and literatures.

Materials	ICE (%)	Cycles / RC (mAh g ⁻¹)	Biggest CD (mA g ⁻¹) / RC	AMR (%)	Ref.
PMo₁₀V₂-ILs@MIL-100	66.94	100 / 1258.5	1000 (or 650 mA cm⁻²) / 600	70	This work
POMs-based anodes					
POM/CNT	34.9	100 / 850	1 mA cm ⁻² / 10	80	2
[MnMo₆O₂₄]⁹⁻/SWNTs	37.8	100 / 932	1 mA cm ⁻² / 10	50	3
Pyrene-Anderson-CNTs	52.7	100 / 665	1 mA cm ⁻² / 10	30	4
Mo₆O₁₈-SCN	51.7	100 / 876	NA	40	5
SiW₁₁- CNTs	49.7	100 / 650	1 mA cm ⁻² / 10	30	6
SWNTs/Py-SiW₁₁	40.8	100 / 580	1 mA cm ⁻² / 10	30	7
NAM-EDAG	63	100/above1000	5000 / 240	80	8
GO-IL-P₂Mo₁₈	62.8	100 / 973	100 / 1000	80	9
PMo₁₀V₂/PDA	-	100 / 915.3	1000 / 300	70	10
MOFs-based anodes					
Li/Ni-NTC	55.2	80 / 482	NA	60	11
Mn-LCP	32.3	50 / 390	NA	80	12
Zn₃(HCOO)₆	52.5	60 / 560	1560 / 20	70	13
Co-BTC-CPs	49.15	100 / 879	2000 / 500	70	14
Fe₂O₃@UTSA-74	-	45 / 650	NA	70	15
Co₂(OH)₂(bdc)	72.8	100 / 650	500 / 10	70	16
Mn-BTC	40	100 / 694	2061 / 10	70	17
Zn(IM)_{1.5}(abIM)_{0.5}	-	200 / 190	400 / 200	70	18
Cu-BTC	42.8	100 / 740	383 / 50	70	19

Asp-Cu	26.6	200 / 233	400 / 100	70	20
MIL-53(Fe)@RGO	42.3	100 / 550	NA	70	21
POMOFs-based anodes					
POMOF-1	50.6	500 / 350	NA	65	22
PMG-3	64.1	100 / 1075	3000 / 400	70	23
NUU-11	61.3	200 / 750	500 / 400	70	24
NENU-507	56.15	100 / 640	NA	50	25
NENU-601	45	200 / 750	500 / 470	60	26
Compound 1	58	100 / 570	NA	70	27

ICE: Initial coulombic efficiency. **RC:** Reversible capacity. **CD:** Current density.

AMR: Active material ratio

Reference

- Y. Dai, Q. Li, S. Tan, Q. Wei, Y. Pan, X. Tian, K. Zhao, X. Xu, Q. An, L. Mai and Q. Zhang, *Nano Energy*, 2017, **40**, 73-81.
- J. Hu, Y. Ji, W. Chen, C. Streb and Y.-F. Song, *Energy Environ. Sci.*, 2016, **9**, 1095-1101.
- Y. Ji, J. Hu, L. Huang, W. Chen, C. Streb and Y.-F. Song, *Chem. Eur. J.*, 2015, **21**, 6469-6474.
- L. Huang, J. Hu, Y. Ji, C. Streb and Y. F. Song, *Chemistry*, 2015, **21**, 18799-18804.
- R. N. Nasim Khan, N. Mahmood, C. Lv, G. Sima, J. Zhang, J. Hao, Y. Hou and Y. Wei, *RSC Adv.*, 2014, **4**, 7374.
- W. Chen, L. Huang, J. Hu, T. Li, F. Jia and Y.-F. Song, *Phys. Chem. Chem. Phys.*, 2014, **16**, 19668-19673.
- D. Ma, L. Liang, W. Chen, H. Liu and Y.-F. Song, *Adv. Funct. Mater.*, 2013, **23**, 6100-6105.
- J. Xie, Y. Zhang, Y. Han and C. Li, *ACS Nano*, 2016, **10**, 5304-5313.

- 9 J. Hu, H. Diao, W. Luo and Y.-F. Song, *Chem. Eur. J.*, 2017, **23**, 8729-8735.
- 10 Y.-H. Ding, J. Peng, S.-U. Khan and Y. Yuan, *Chem. Eur. J.*, 2017, **23**, 10338-10343.
- 11 X. Han, F. Yi, T. Sun and J. Sun, *Electrochim. Commun.*, 2012, **25**, 136-139.
- 12 Q. Liu, L. Yu, Y. Wang, Y. Ji, J. Horvat, M.-L. Cheng, X. Jia and G. Wang, *Inorg. Chem.*, 2013, **52**, 2817-2822.
- 13 K. Saravanan, M. Nagarathinam, P. Balaya and J. J. Vittal, *J. Mater. Chem.*, 2010, **20**, 8329-8335.
- 14 C. Li, X. Lou, M. Shen, X. Hu, Z. Guo, Y. Wang, B. Hu and Q. Chen, *ACS Appl. Mater. Interfaces*, 2016, **8**, 15352-15360.
- 15 C. S. Yan, H. Y. Gao, L. Le Gong, L. F. Ma, L. L. Dang, L. Zhang, P. P. Meng and F. Luo, *J. Mater. Chem. A*, 2016, **4**, 13603-13610.
- 16 L. Gou, L.-M. Hao, Y. X. Shi, S.-L. Ma, X.-Y. Fan, L. Xu, D.-L. Li and K. Wang, *J. Solid State Chem.*, 2014, **210**, 121-124.
- 17 S. Maiti, A. Pramanik, U. Manju and S. Mahanty, *ACS Appl. Mater. Interfaces*, 2015, **7**, 16357-16363.
- 18 Y. Lin, Q. Zhang, C. Zhao, H. Li, C. Kong, C. Shen and L. Chen, *Chem. Commun.*, 2015, **51**, 697-699.
- 19 S. Maiti, A. Pramanik, U. Manju and S. Mahanty, *Microporous Mesoporous Mater.*, 2016, **226**, 353-359.
- 20 C. Zhao, C. Shen and W. Han, *RSC Adv.*, 2015, **5**, 20386-20389.
- 21 C. Zhang, W. Hu, H. Jiang, J.-K. Chang, M. Zheng, Q.-H. Wu and Q. Dong, *Electrochim. Acta*, 2017, **246**, 528-535.
- 22 Y. Yue, Y. Li, Z. Bi, G. M. Veith, C. A. Bridges, B. Guo, J. Chen, D. R. Mullins, S. P. Surwade, S. M. Mahurin, H. Liu, M. P. Paranthaman and S. Dai, *J. Mater. Chem. A*, 2015, **3**, 22989-22995.
- 23 T. Wei, M. Zhang, P. Wu, Y.-J. Tang, S.-L. Li, F.-C. Shen, X.-L. Wang, X.-P. Zhou and Y.-Q. Lan, *Nano Energy*, 2017, **34**, 205-214.
- 24 Q. Huang, T. Wei, M. Zhang, L.-Z. Dong, A. M. Zhang, S.-L. Li, W.-J. Liu, J. Liu and Y.-Q. Lan, *J. Mater. Chem. A*, 2017, **5**, 8477-8483.

- 25 Y.-Y. Wang, M. Zhang, S.-L. Li, S.-R. Zhang, W. Xie, J.-S. Qin, Z.-M. Su and Y.-Q. Lan, *Chem. Commun.*, 2017, **53**, 5204-5207.
- 26 X. X. Li, F. C. Shen, J. Liu, S. L. Li, L. Z. Dong, Q. Fu, Z. M. Su and Y. Q. Lan, *Chem. Commun.* , 2017, **53**, 10054-10057.
- 27 X.-Y. Yang, T. Wei, J.-S. Li, N. Sheng, P.-P. Zhu, J.-Q. Sha, T. Wang and Y.-Q. Lan, *Inorg. Chem.*, 2017, **56**, 8311-8318.